8th U. S. National Combustion Meeting
Organized by the Western States Section of the Combustion Instituteand hosted by the University of Utah
May 19-22, 2013

Time-Resolved 3D OH Planar Laser-Induced Fluorescence System for Multiphase Combustion

Kevin Y. Cho[1], Aman Satija[1], Timothée L. Pourpoint[2], Steven F. Son[1], Robert P. Lucht[1]

[1]Department of Mechanical Engineering, Purdue University, West Lafayette IN 47906 USA
[2]Department of Aeronautics and Astronautics Engineering, Purdue University, West Lafayette IN 47906 USA

Imaging dynamic multiphase combusting event is challenging. Conventional techniques can image only a single plane of an event, capturing limited details. Here, we report on a three-dimensional, time-resolved, OH planar laser-induced fluorescence (3D OH PLIF) technique that was developed to measure the relative OH concentration in multiphase combustion flow fields. The technique involves rapidly scanning a laser sheet across a flow field of interest. The overall experimental system consists of a 5 kHz OH PLIF system, a high speed detection system (image intensifier and CMOS camera) and a galvanometric scanning mirror. The scanning mirror was synchronized with a 500 Hz triangular sweep pattern generated using Labview. Images were acquired at 5 kHz corresponding to 5 images per mirror scan, and 1000 scans per second. This result in essentially a 3D volumetric data obtained with a spatial resolution of 500×500×5 voxels mapped to a field of interest covering 30×30×8 mm^3. Droplet combustion of methanol gelled with hydroxypropyl cellulose (3 wt.%, 6wt.%) was the main focus of the study. The resulting 3D data show a comprehensive view of jetting events in gelled droplet combustion that was not observed with high-speed imaging or 2D OH PLIF. Fireballs from jetting events that were assumed to be detached from the flame sheet using 2D OH PLIF were observed to be attached to the flame sheet with a thin stretched flame. Flame standoff distance, flame sheet thickness, position and speed of jets could be measured with less uncertainty. The temporal and spatial resolution was sufficient to view the dynamic events in great detail in the multiphase combustion flow field. The previous jet speed analysis work with 2D OH PLIF is compared with the measurement from 3D OH PLIF and found to be reasonably close. The system is limited by the repetition rate of the pulsed laser; any combustion flow field with a frequency of interest over 500Hz would not be resolved.

1. Introduction

Most non-intrusive optical diagnostics of flames are 1D or 2D measurements. Examples are particle imaging velocimetry (PIV), Raman spectroscopy, coherent anti-stokes Raman spectroscopy, (CARS), and planar laser induced fluorescence (PLIF). However, flames that involve turbulence, or other complex phenomena such as transient jetting, are 3D events. In turbulent combustion regimes with asymmetrical and random flame structures, using 1D or 2D diagnostic techniques will yield only part of the full picture. A 3D optical measurement using rapidly sweeping PLIF laser sheet was conceptualized and demonstrated in the late 1980s [15]. However, it was not practical due to the low temporal and spatial capabilities at the time. With the advances in laser and detection technologies, 3D measurements of transient plumes structures and liquid interfaces were made in the last two decades [5]. Still, 3D measurement of flame structure using OH or CH concentration is very challenging, because high frequency pulsed lasers are required instead of continuous wave lasers.

The propulsion community is interested in gelled fuels (or propellants) because of potential safety and performance benefits. Gelled fuel droplet combustion events consist of microexplosions, which make the flame structure random, dynamic, and asymmetric [21]. Deeper understanding of gelled fuel droplet combustion is needed to improve models and simulations, which will result in better engine designs.

The objective of this work is to develop, characterize, and use 3D OH PLIF to image gelled fuel droplet combustion.

A. OH PLIF

The OH radical is one of the most important intermediates in combustion [13], and is widely used for determining flame front locations [3, 18]. In OH PLIF, a planar laser sheet is transmitted through a flow field at a wavelength of approximately 283 nm. The laser frequency is tuned to excite a selected transition in the OH molecule to a higher electronic level. The OH molecule fluoresces near 310 nm, which is captured with a UV-sensitive camera.

Previous laser imaging experiments had limited ability to visualize fast transient events due to the low repetition rate of the laser and acquisition devices. Mercier et al. used OH PLIF at 3 Hz to visualize the flame front around an acetone droplet [17]. Kaminski et al. achieved higher repetition rates with multiple 10 Hz lasers but they could only collect sequences of eight images [13]. Similarly, Hult et al. used a burst system of 33 kHz OH PLIF with particle image velocimetry (PIV) on turbulent jet diffusion flames, but were limited to six images [12].

With recent improvements in the laser and imaging technology, multi-kilohertz pulsed lasers with sufficient energy and high-speed intensifiers have become available for OH PLIF. For example, Paa et al. performed 1 kHz PLIF formaldehyde PLIF in a spray combustion reactor [20]. Boxx et al. [3] performed 5 kHz OH PLIF with simultaneous PIV on lifted jet flames and swirl stabilized flames. These measurements showed dynamic flame stabilization events, such as local ignition/extinction, liftoff, and flashback. Hedman et al. used 5 kHz OH PLIF system on a bimodal ammonium perchlorate (AP) and hydroxyl-terminated polybutadiene (HTPB) propellant combustion [9-11]. The 5 kHz OH PLIF system was used to measure the crystal diameter (from AP fluorescence) and the flame simultaneously.

B. 3D OH PLIF

One of the drawbacks of PLIF systems is that events out of the plane of the laser sheet are not captured. That can be overcome by sweeping the laser sheet with sufficiently high speed. The movement of the reflecting mirror can be achieved by electromechanical, electro-optic, or acousto-optic devices. The reflection can occur with oscillating mirror, rotating polygon mirror, or rotating prism [7]. Since the camera optics are static and the object distance is changing constantly, the depth of field of the imaging device needs to be greater or equal to the distance between the farthest imaging planes for good image quality. For gas flow with frequency of interest of f_1, the image acquisition rate needs to be at least $2\times f_1$. For three-dimensional structure with P_n, or the number of planes to be recorded, acquisition rate needs to be at least $2\times f_1\times P_n$. The fluorescence life time should be not more than $1/(2f_1)$ to prevent smearing of images [8]. For many turbulent flows, the acquisition rate needs to be 100 kHz to 3 MHz to 'freeze' the 3D image of turbulent gaseous flows [15]. Although 3D PLIF has been conceptualized and demonstrated as early as 1987 by Kychakoff et al. [15], the rates at which the planar laser can be detected were limited by the lasers and detectors. At that time, lasers with enough pulse energy had 10-500Hz of repetition rate; solid state detectors were limited by the rate of about 10^7 pixels per second (i.e. 512×512 arrays at 40 Hz, 100×100 arrays at 1 kHz, etc.); intensified detectors were limited to few kilohertz [8].

With improvements in laser and detection technologies, 3D PLIF (or other 3D optical techniques) have become more applicable. Crimaldi et al. in 2001 [6] used electromechanical optical scanner with argon-ion laser to scan turbulent plume structure with PLIF. The temporal resolution was 1000 Hz and the spatial resolution was 150 μm. Wellander et al. [25] in 2011 obtained 3D images of plumes using Mie-scattering technique. Continuous wave Nd: YAG laser of 20 kHz repetition rate with two oscillating mirrors were used to obtain 610×512×20 voxels (3D pixels) at 3D repetition rate of 1000 Hz. Other examples of 3D PLIF work are Unger et al. [23], Tian et al. [22], Vliet et al. [24], and Deusch et al. [7].

C. Gelled fuel droplet combustion

Gelled propellants are of significant current interest due to potential safety and performance benefits compared with neat and solid propellants. Gelled propellants are designed to behave like solids under low stress and like liquids under high stress. Because of the high viscosity of gelled propellants under storage condition, energetic particles can be suspended in the gels, increasing the energy density while maintaining homogeneity. Because shear-thinning gelled propellants do not flow under low stress, the safety of hypergolic and/or toxic liquids is increased when they are in gelled form. Gels still maintain the flexibility of the liquid propellants because for some gels,

viscosity decreases close to that of the liquid when forced through an orifice at high pressure. Its liquid-like behavior gives the flexibility to throttle and restart in engines [19].

Despite their potential advantages, gelled propellants have more complex rheology and burning characteristics than liquid propellants. Combustion parameters such as the heat of vaporization, burning rate, and ignition delay time depend on the type and quantity of the gellant [2]. Analyzing a single droplet burning process for a gelled propellant is important for the overall modeling of spray combustion of rocket engines and to gain insight into the mechanisms of combustion. By studying processes such as mixing, heating, and vaporization of a droplet, deeper fundamental understanding of gelled propellant combustion can be achieved. This will enhance the predictive capabilities for rocket engines with gelled propellants.

Although part of a gelled fuel droplet combustion process can be described by the D^2 law, deviations can be observed with increased gellant content [1]. Gelled fuel droplet combustion is similar to slurry droplet combustion, because a layer of less volatile component (unburned gellant) can remain on the outside after the fuel is vaporized and burned [19]. This is due to the difference in evaporation temperatures of fuel and gellant. The layer of gellant accumulates, forming an outer shell which hinders vapors from escaping freely. The nature of the outer shell is different for different gellant types, which causes drastically different microexplosions. For typical organic gels made with cellulose derivatives and polymers, the outer shell of the droplet becomes an elastic layer of highly viscous gellant [14]. The elastic nature of the outer shell can cause the droplet to bubble with trapped vapor, and swell [21]. When the pressure of the trapped fuel vapor exceeds the tensile stress of the viscoelastic shell, the shell bursts, releasing a jet of fuel vapor [14]. The tensile stress of the outer shell that forms during combustion has not been measured experimentally, but with reasonable assumptions, it can be estimated to be on the order of 2 MPa [14]. The process of bubbling, swelling, and bursting happens throughout the droplet combustion process, and in the end, the organic gellant is consumed [21]. The outer shell thickness is theorized to be higher with larger initial droplet diameter [14].

Past work with 2D OH PLIF included identifying different types of jetting events, and quantifying the jet speed for the different types of jets [4]. Three types of jets were identified and distinguished for the first time: (1) jets that distort the flame front, (2) jets that break the flame front, and (3) jets that form a fire ball outside of the flame front. The average jet speed was the highest for the third type, and the lowest for the first type [4]. A broken flame front is believed to be caused by high shear rate from the vapor jets, which is analogous to local flame extinction in non-premixed turbulent jet combustion [4].

2. Experimental System

A. Laser and detection system

A Sirah Credo (CREDO-DYE) dye laser was pumped using an Edgewave Nd: YAG (IS811-DZ) solid state laser. The Nd: YAG operated at 532 nm delivering 6 mJ per pulse at 5 kHz with an 8 ns pulse duration. In addition to an oscillator and a pre-amplifier in a single dye cell, the dye laser was equipped with a main amplifier (Brewster dye cell) that further increased the pulse energy of the output beam. The Rhodamine 590 dye concentrations in the oscillator and amplifier were 0.135 g/l and 0.09 g/l respectively; the dye solvent was 100 % ethanol. Due to the high pulse frequency, two 4 liter capacity dye pumps were used to avoid rapid bleaching of the dye. One pump supplied the oscillator cell while the other supplied the amplifier cell. The dye was cooled using an external chiller (HALCO Products Company, 76607P) that supplied cooled water at 13.25 l/min. The dye laser was tuned to 566.44 nm. This visible beam was focused into a frequency doubling crystal to produce an ultraviolet beam at 283.22 nm. After the frequency doubling, a compensator was used to direct the beam into a four prism separator for isolation of the ultraviolet beam from the visible beam.

With the maximum pump energy of 6 mJ, the energy of the output dye laser was 0.4 mJ, or 2.0 W of average power at 5 kHz. The laser wavelength was adjusted to excite the $Q_1(7)$ line at 283.222 nm. The wavelength of the 586.44 nm beam was measured using a High Finesse wavelength meter (WS6 Precision). The details of laser optics will be discussed in the next section. OH fluorescence was detected near 310 nm as discussed below.

To transmit the fluorescence signal to the detection system, a UV-grade lens from UKA Optics (UV1054B 105 mm F/4.0 Quartz Lens) was used. A Semrock interference filter (FF01-320/40-25) with transmission of 74 % at 310 nm was used to selectively detect OH fluorescence and block scattered laser light at 283 nm. The lens was mounted

to a Video Scope International high speed image intensifier (VS4-1845HS). The intensifier is capable of operating at rates as high as 100 kHz with a gain of up to 80,000. The intensifier was gated at 80 ns and gain was set to 70,000. A Vision Research Phantom 7.3 color high speed camera was connected to the output of the image intensifier. The high speed camera can operate up to 6688 fps at full resolution of 800×600 with 16 bit image depth. The camera system was positioned perpendicular to the direction of the laser propagation and the plane of the laser. The depth of field of the camera was approximately 1.6 cm. The experimental configuration is shown in Fig. 1.

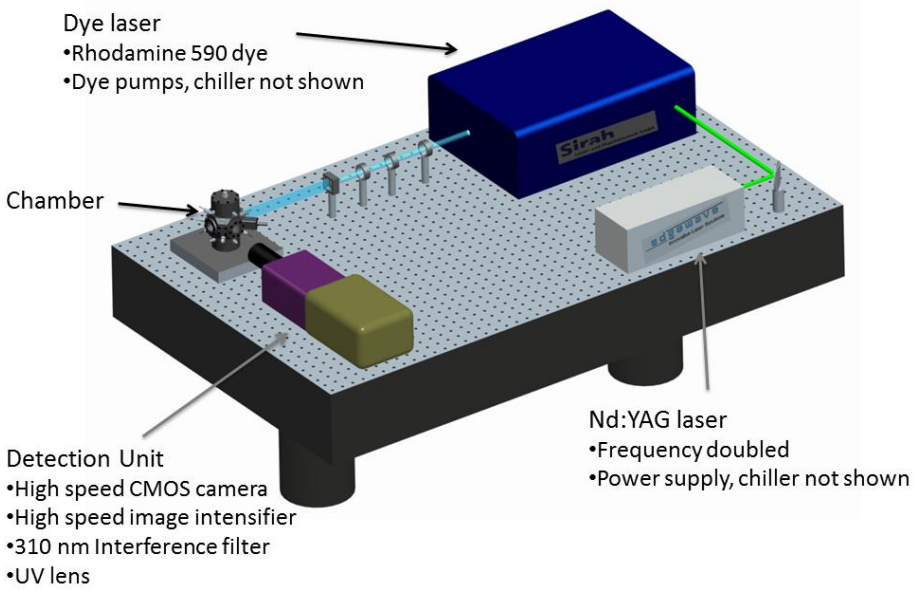

Fig. 1 Schematic diagram of the experimental system.

B. Galvanometric mirror system

Electromechanical servo with coated silicon mirror substrate was used to oscillate reflection of the laser beam. A single axis servo driver amplifier (67122H-1, Cambridge Technology) was used to provide communication with Labview and provide power and control to the galvanometer scanner (6220HM40B, Cambridge Technology). Silicon mirror substrate (D04781, Cambridge Technology) with clear aperture of 8 mm was chosen. Although the default aluminum coating has good reflectivity for continuous wave lasers, it would undergo ablation under high peak power of a nanosecond laser. Uncoated silicon mirror substrates were custom coated for 283 nm laser beam at Lattice Electro Optics with 99.95% reflectivity. The galvanometer scanner had rated angular excursion of 40°, rotor inertia of 0.125 gm·cm^2, back EMF voltage of 108 μV/deg·s, small angle step response of 200 μs. It has a closed loop position detector that can output position signal of the servo without start-up calibration.

Two optics were used downstream of the rotating mirror. A positive spherical lens (f_2 = 500 mm, C.A. = 50 mm) was positioned at distance f_2 from the rotating mirror to get parallel beams. The beam waist was located at distance f_2 from the positive spherical lens, and a flow field of interest was located there. To obtain a collimated laser sheet, negative cylindrical lens (f_1 = -50 mm, C.A. = 25 mm) was located at distance f_1 from the rotating mirror. Fig. 2 schematically portrays the top view of the laser system, rotating mirror, and laser optics.

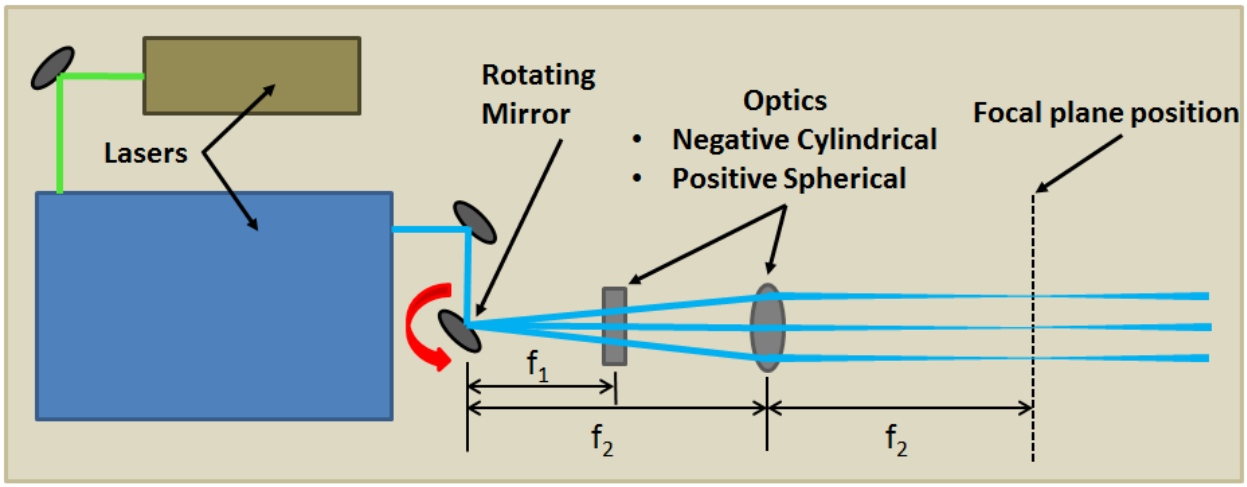

Fig. 2 Top view of the 3D OH PLIF setup.

A Labview code was written to input a triangle wave to the controller with given frequency, offset, and phase. Input signal from Labview, output signal from the galvanometric controller, camera sync pulse, and camera trigger pulse was fed into an oscilloscope (Tektronix DPO 4034). Oscilloscope data acquisition rate of at least 500 kHz was required to accurately capture the TTL signal from the camera. Input and output signals were out of phase because the galvanometric mirror system had a finite response time, and camera sync pulse did not coincide with the edge of each sweep. To have repeatable position between experiments and capture images at the edge of each sweep, phase input was changed until edge of the triangular position was close to the camera sync pulse. An example of position and camera sync signal is shown in Fig. 3. A MATLAB script was written to identify the peak of each TTL pulse and its time. The mirror position at that instance of TTL pulse was identified. A position vs. image number is plotted in Fig. 4.

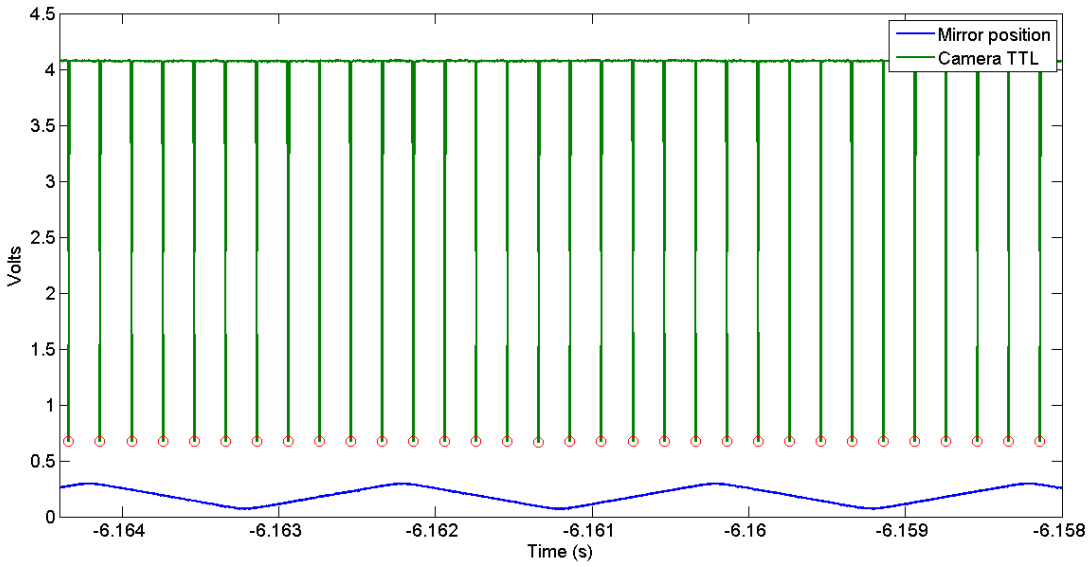

Fig. 3 Camera sync pulse (green) and galvanometric mirror position (blue). Time 0 indicates the instance of trigger.

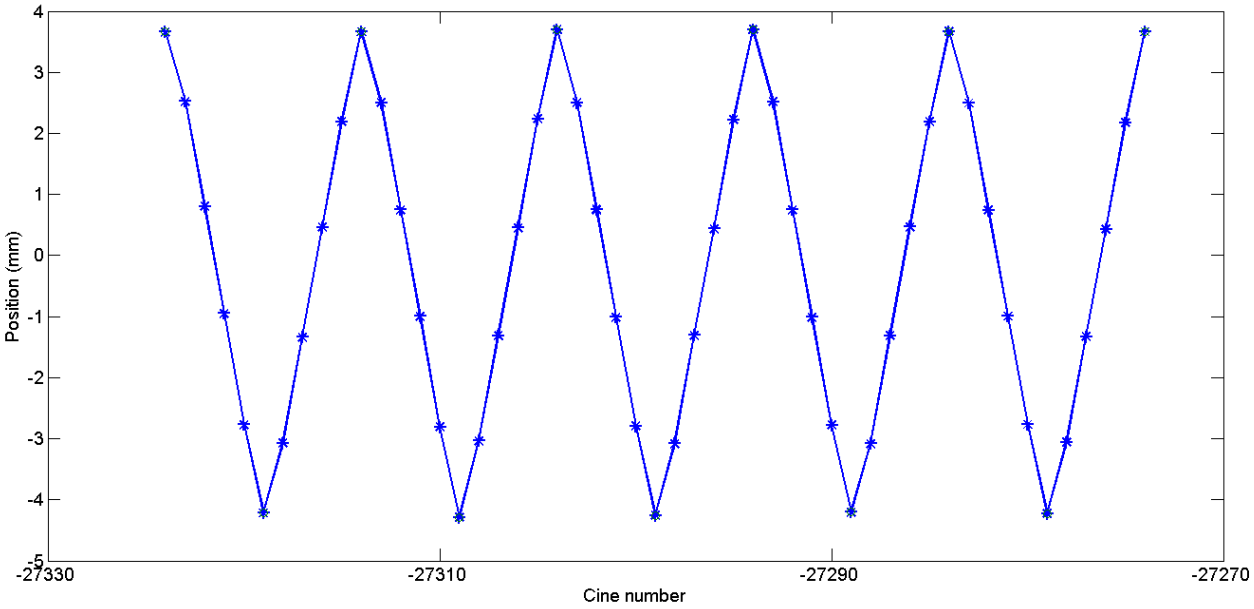

Fig. 4 Position of the image plane for each image number.

The position input signal, position output signal, and the actual position in the flow field were calibrated. A business card with a pinhole was attached to a micrometer stage, and placed in the beam waist. The frequency was set to zero, and the laser sheet was moved by a small increment by changing the offset. The micrometer stage was adjusted until part of the laser sheet went through the center of the pinhole. The input voltage, the position output voltage, and the actual position was recorded for the range of interest. A linear fit was used, and the fit equation was used during post processing in MATLAB. The sweep distance of the laser sheet was about 8-8.5 mm, ranging from edge of the flame to 1-2 mm beyond the center of the droplet. The mirror was oscillated at 500 Hz, or 1000 sweeps per second, generating five new slices per sweep, which makes 3D time resolution 1 ms.

C. Sample preparation and method

The methanol used in this study was acquired from Macron chemicals (methyl alcohol, anhydrous, ChromAR®, 99.9% purity). Klucel ® HR hydroxypropyl cellulose (HPC) from Hercules was used as a gellant. HPC dissolves in methanol, so they were mixed by hand and allowed to disperse throughout the liquid for a week. The mixture was stirred twice during the span of a week to break clumps of HPC [14]. Samples with 3 wt.% and 6 wt.% HPC were prepared (±0.01%). Gelled fuel droplets were suspended on a quartz rod with a thickness of 2 mm (±0.4 mm). Droplets had initial diameter of 4.8 mm (±0.8 mm). The droplets were lighted with a butane torch in 1 atm in room temperature.

3. Results & Discussion

A significant challenge with this 3D data is analyzing and presenting the results. Images and data from the oscilloscope were post processed in MATLAB. The MATLAB code was written to present the 3D data in four different ways. Two of the methods will be used to show the data in the paper, while all methods will be shown in the oral presentation. One of the two methods shown in this paper involves showing all planes simultaneously. In this method, the x-axis is scaled to be larger than the y and z-axis so that all images can be shown. The x-axis is the direction of the laser sheet movement, which is much smaller than the width and height of the image. The other method uses the isosurface function in MATLAB to connect pixels with the same pixel value, creating 3D surfaces. An arbitrary pixel value that best describes the flame is chosen.

All gelled droplets burn steadily like the liquid counterpart in the beginning of combustion. Fig. 5 shows steady combustion of 3 wt.% HPC methanol gelled fuel droplet. In all subsequent plots, the laser is going in the direction of decreasing y-axis, laser is sweeping in direction of x-axis, and the camera is pointing towards decreasing x-axis.

Partial OH signal is missing in Fig. 5a) because the droplet blocks the laser sheet. The Fig. 5a) shows a single sweep, containing six images at different locations, and Fig. 5b) shows 3D isosurface with surface value of 330. In the Fig. 5b) the inner and outer surface of the OH signal can be seen. The flame standoff distance and flame thickness can be calculated from the 3D data. The 3D OH PLIF has an advantage over 2D OH PLIF when viewing steady flames because a static laser sheet may not coincide with the center of the droplet. Uncertainty is reduced by sweeping the laser sheet from edge of the flame to a few millimeters beyond the center of the droplet. When microexplosions start to occur, the flame structure is highly asymmetrical and random. Fig. 6 shows a flame structure of 6 wt.% HPC methanol gel between microexplosions. This is a typical example of how the flame looks at these times.

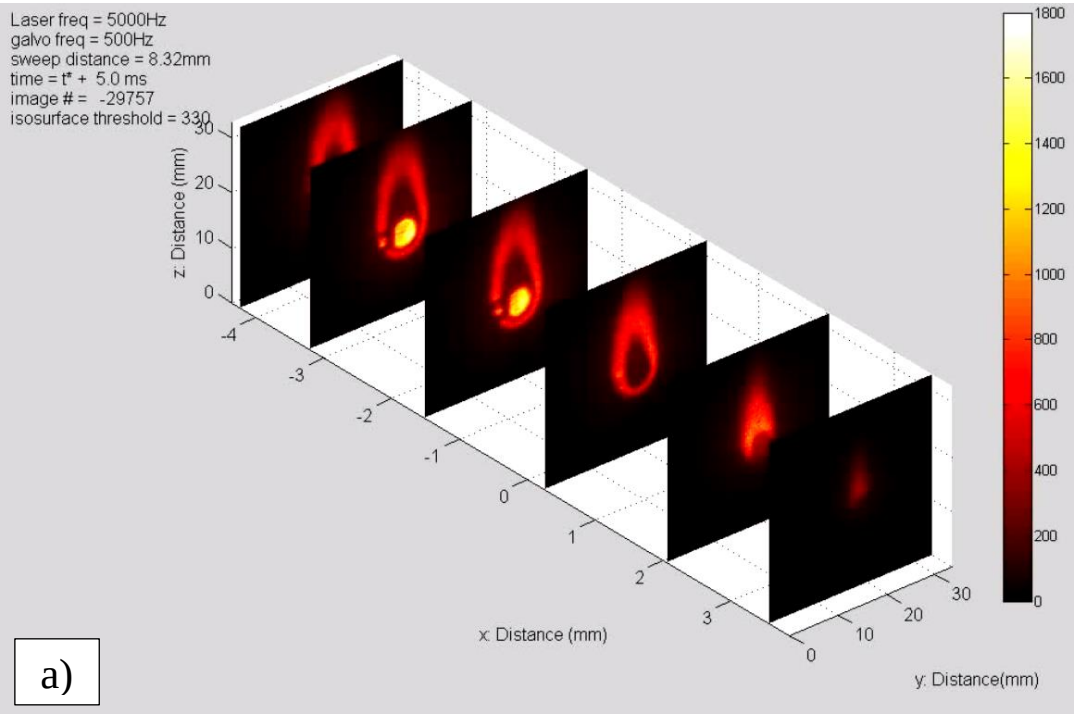

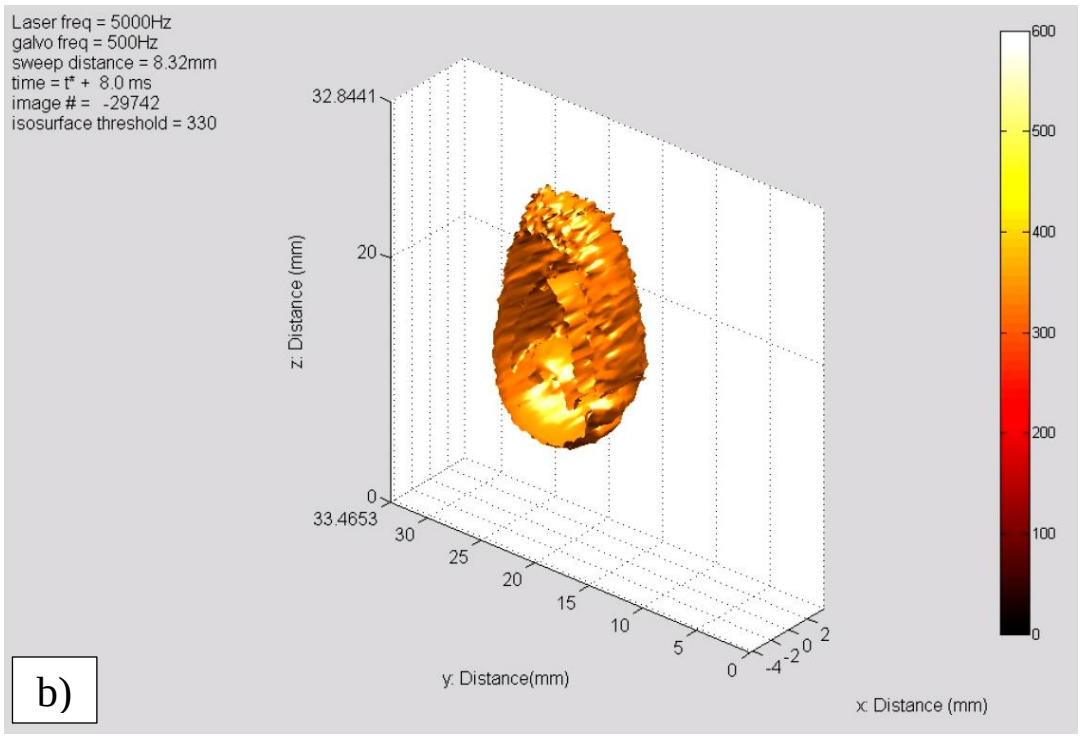

Fig. 5 a) Steady combustion of 3 wt.% HPC methanol gel in 1 atm, 6 slices. b) Isosurface construction at surface value of 330.

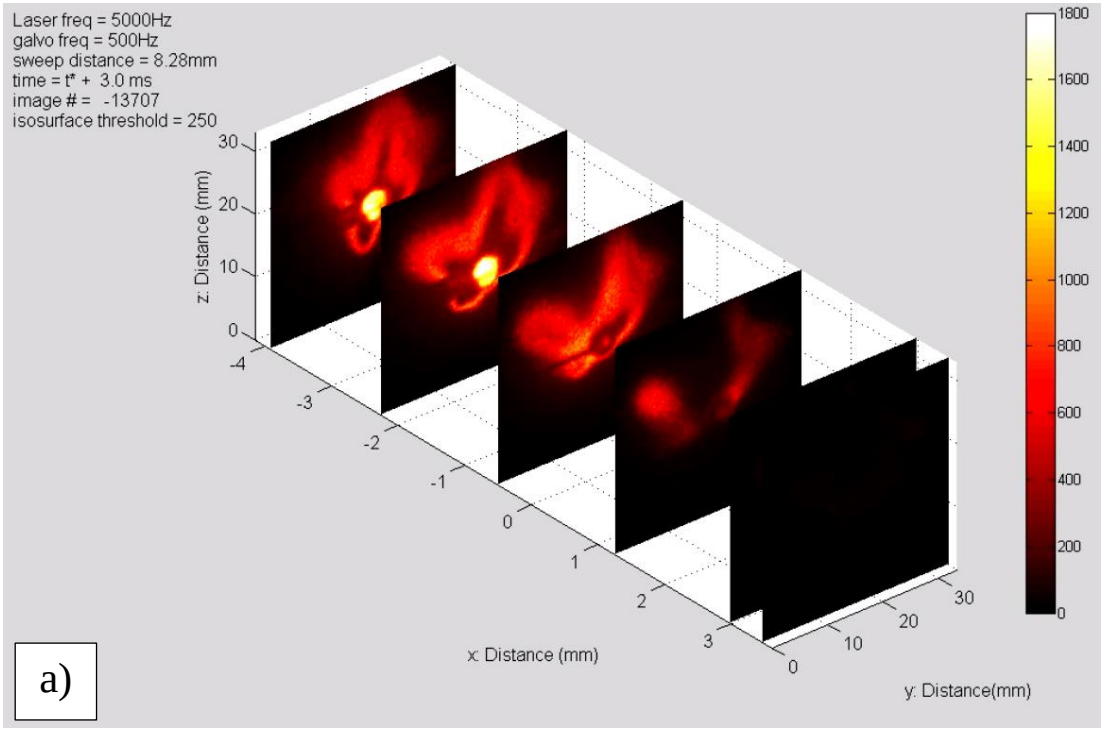

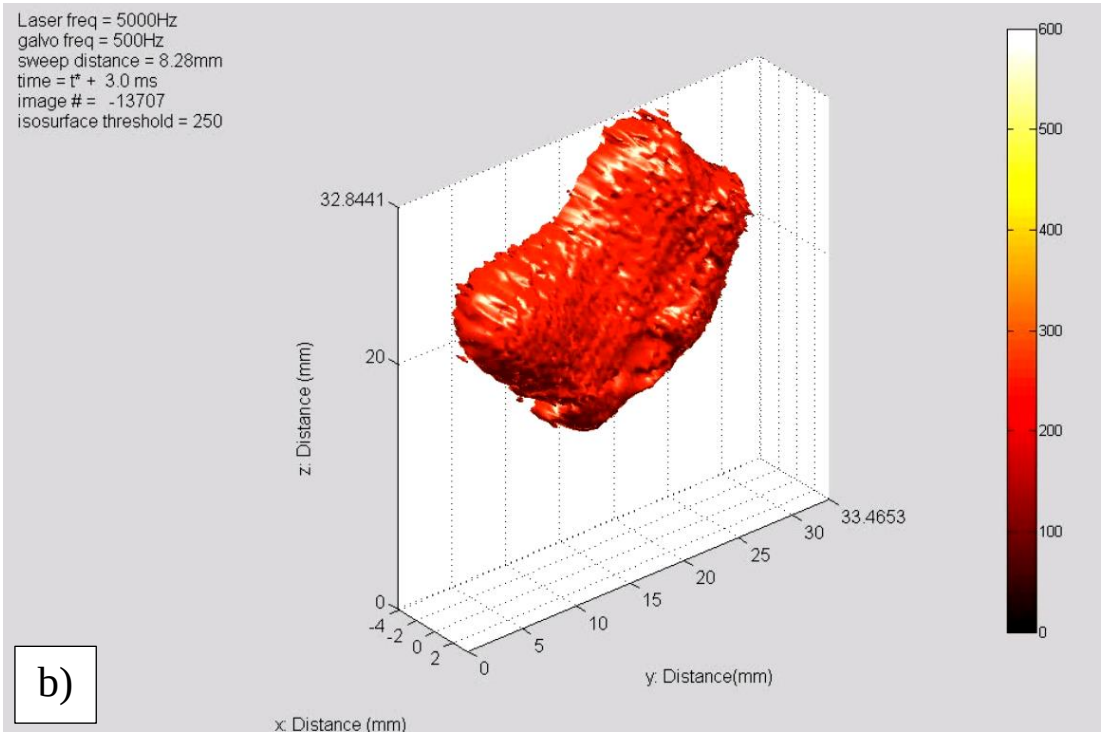

Fig. 6 Flame structure of 6 wt.% HPC methanol gel between microexplosions. a) Six images displayed simultaneously. b) A 3D isosurface at surface value 250.

When jetting events occur, it produces high speed fuel vapor jets that are often strong enough to distort and break the flame sheet. In this process, flame is stretched in a curved shape, and discontinuity in the OH signal is observed. An example from 3 wt.% HPC methanol gelled droplet combustion is shown in Fig. 7. In Fig. 7a), discontinuity of the OH signal can be seen in slices at $x \approx -2.4$mm and $x \approx -0.7$mm. This is also observed in the isosurface, shown in Fig. 7b). The 1 ms 3D temporal resolution was enough to view the dynamic event. A sequence of the isosurface plot is shown in Fig. 8, which is from the same jetting event in Fig. 7. In 2D OH PLIF, this could be captured with 5 times the time resolution of 3D OH PLIF. However, it is expected that some jetting events with local extinctions were identified as regular jetting events in 2D OH PLIF because the discontinuity may not have occurred at the static laser sheet.

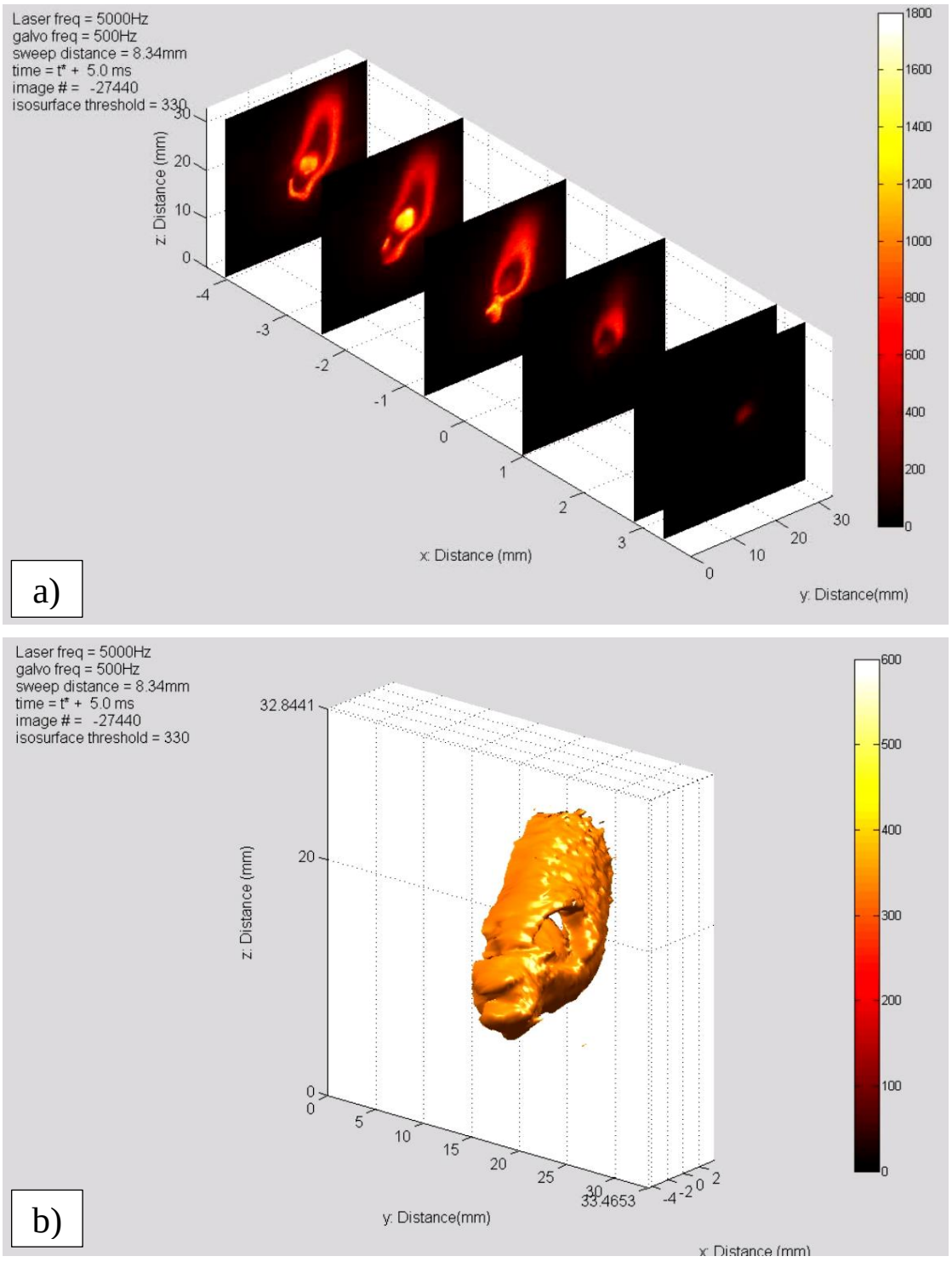

Fig. 7 Jetting event with broken flame front from 3 wt.% HPC methanol gelled droplet combustion. Discontinuity in the OH signal can be seen. a) 6 slices from the sweep displayed simultaneously. b) Isosurface with surface value of 330.

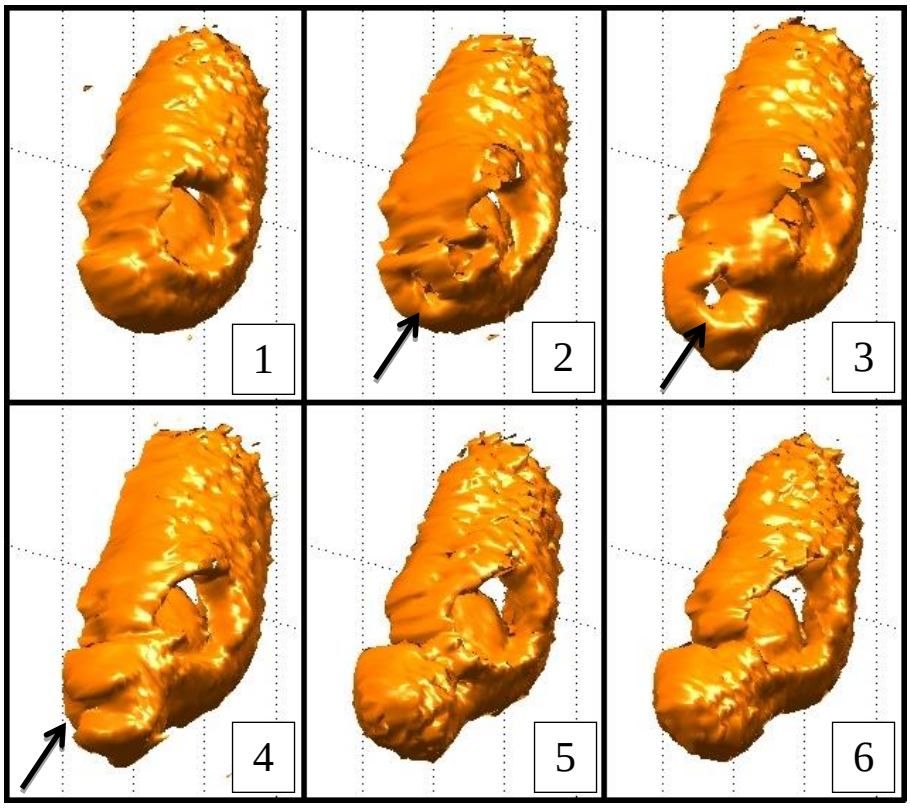

Fig. 8 Jetting event of 3 wt.% HPC methanol gelled droplet. Isosurface value of 330 is shown in 1 ms intervals. Arrow indicates discontinuity in the OH signal, which signifies broken flame front.

Previous work showed that with higher velocity, fire ball formation outside the flame front can occur [4]. This is caused by unburned fuel vapor passing through the broken flame, and burning outside the flame front. An example of this case from 6 wt.% HPC methanol gelled droplet combustion is presented in Fig. 9. From the previous work with 2D OH PLIF, it was believed that the fireball was completely detached from the flame sheet. That would also appear to be the case if a single slice at $x \approx -4.2$mm is viewed in Fig. 9a). However, images from other planes indicate that the fireball is actually attached to the flame sheet with a thin, highly stretched flame. Fig. 10 shows a sequence of a jetting event with fireball formation from 3 wt.% HPC methanol gelled droplet combustion. Fig. 9 and Fig. 10 are from separate experiments. The 3D time resolution was sufficient enough to view the dynamic event.

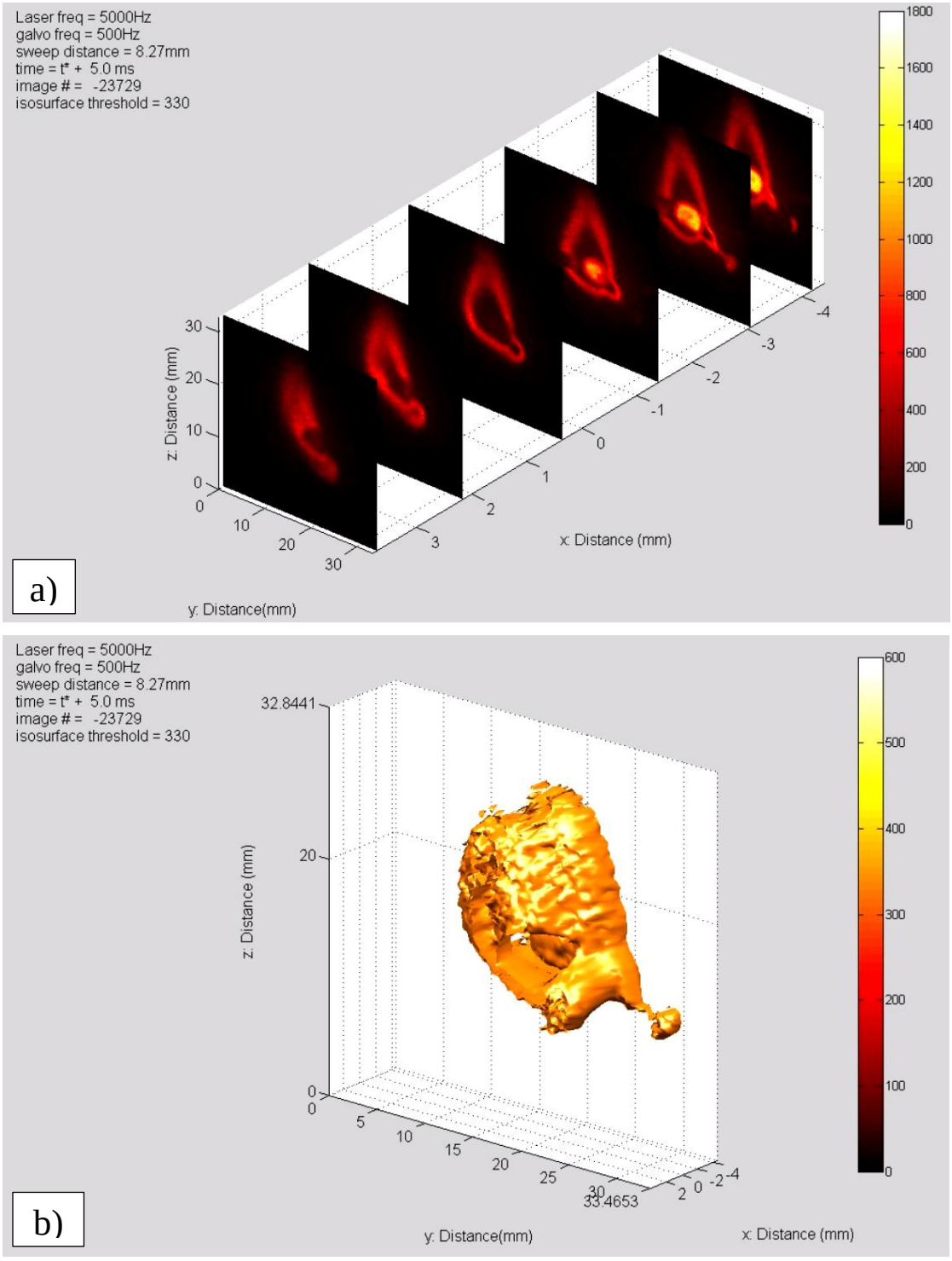

Fig. 9 Jetting event with fireball formation from 6 wt.% HPC methanol gelled droplet combustion.

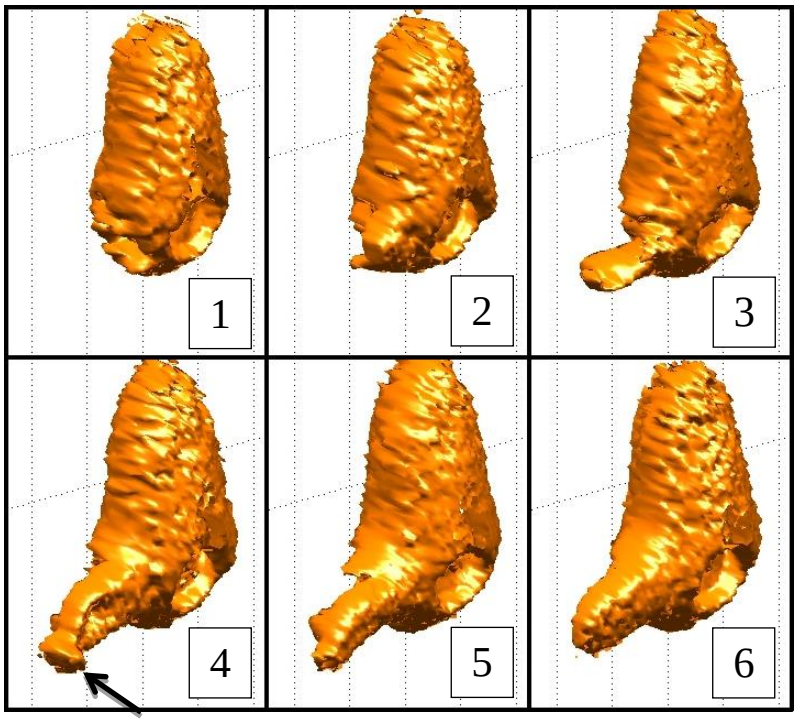

Fig. 10 Jetting event with fireball, from 3 wt.% HPC methanol gelled droplet combustion. Six 3D isosurface plots with value of 330 are shown in 1 ms interval. 'Fireball' can be seen on 4), indicated by an arrow.

The 3D OH PLIF enables visualization of jetting events toward the camera. This gives a high resolution cross section image of the stretched flame. Cross section images of jetting events occurring in the direction of the laser will give limited spatial resolution, because resolution in the x direction is approximately 1 mm, while resolution in y and z-axis is approximately 0.08 mm. Fig. 11 shows an isosurface with tunnel-like structure created by inner and outer OH signals.

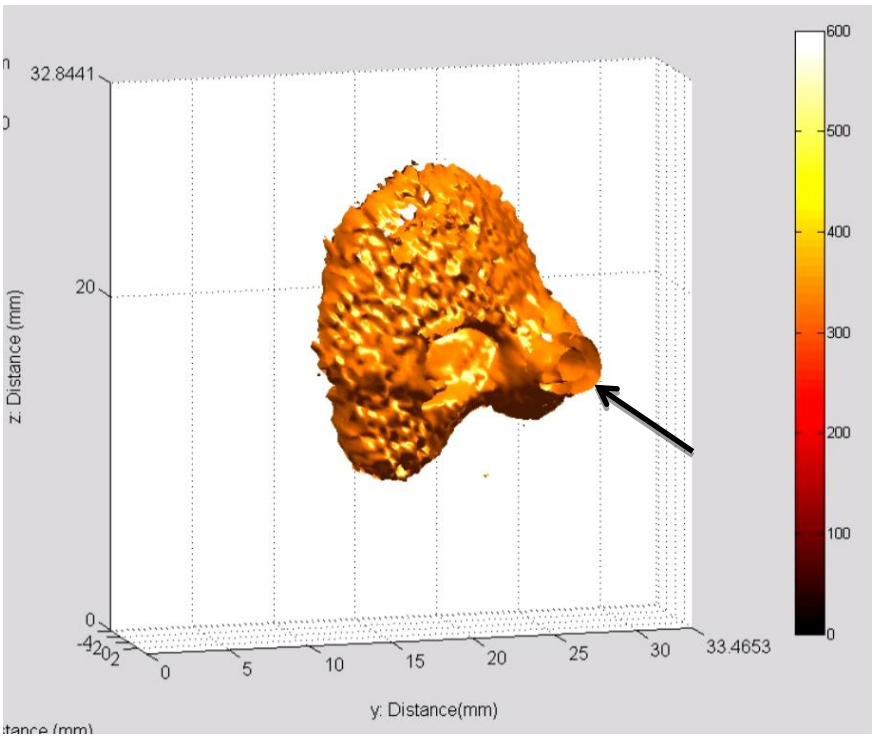

Fig. 11 Jetting towards the direction of sweep (x-axis) which results in 'tunnel' like structure. Data from 6 wt.% HPC methanol gelled droplet combustion.

There was some additional uncertainty from previous work with jet speed statistics because the measurements were made from 2D images [4]. With the 3D structure, more accurate measurement of jet velocity can be made. By tracking x, y, and z coordinates of flame curvature, speed of jets were calculated. Two similar jetting events that form a fire ball, one from 3 wt.% and one from 6 wt.% HPC, were chosen. For 3 wt.%, the average speed over a 3 ms duration was 2.8 m/s, and for 6 wt.%, the average speed over an 1 ms duration was 7.5 m/s. There is a good agreement between the jet speeds from the 3D data and previous 2D OH PLIF studies by Cho et al. [4], illustrated in Fig. 12. Although the fuel is different, the jet speed is expected to be similar and have similar trends. This is because the jet speed is primary driven by the pressure difference created by trapped vapor, which is caused by the elasticity of the gel. Since gelling agents are the same, they are expected to have similar rheology.

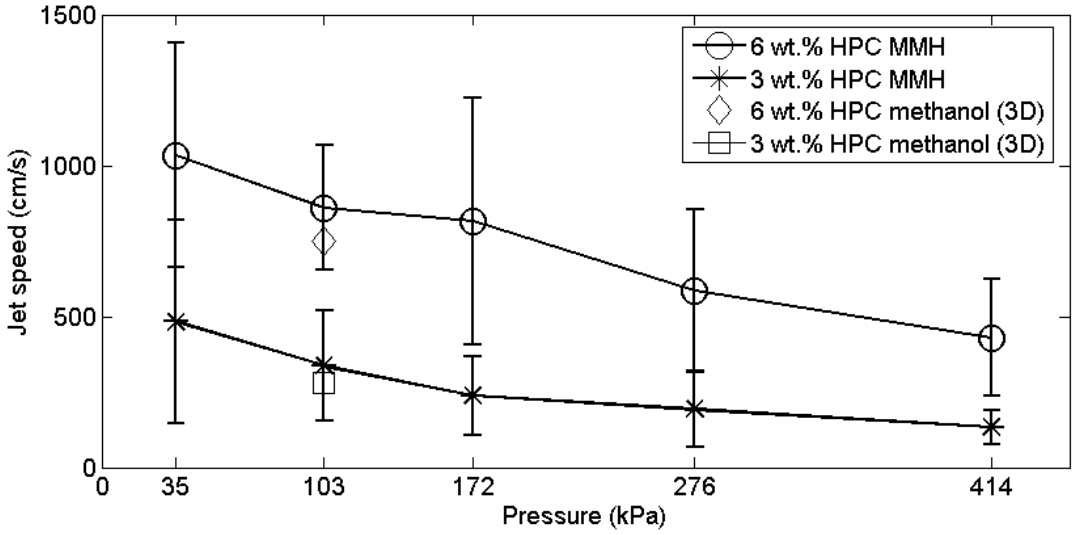

Fig. 12 Average jet speed of HPC/MMH gelled droplet combustion over range of pressures, measured from 2D OH PLIF images. Markers indicate the average speed, while the error bars indicate ±σ of the distribution [4]. Jet speed measurements of HPC/methanol from 3D OH PLIF data are also shown.

The flame disruption, breaking, and formation of flame ball in jetting events are analogous to phenomenon in non-premixed turbulent combustion. The flame stretching, local flame extinction (or quenching), and formation of flame pockets are commonly reported in non-premixed turbulent combustion [16]. In order to utilize models developed for turbulent combustion, parameters such as Reynolds number and Damköhler number need to be calculated. Adapting the turbulent combustion models will aid in determining the criterion for local quenching and pocket formation in gelled droplet combustion.

The Reynolds number is defined as,

$$\mathrm{Re} = \frac{\rho v L}{\mu}. \qquad \text{Eq. 1}$$

This equation can be applied to jetting events, where ρ is density of vapor near the flame temperature, v is velocity of the jet, L is the length of the flame stretch, and μ is the dynamic viscosity of the vapor near the flame temperature.

The Damköhler number is defined as,

$$\mathrm{Da} = \left(\frac{l_0}{l_L}\right)\left(\frac{S_L}{v}\right). \qquad \text{Eq. 2}$$

This equation can be applied to jetting events, where l_0 is integral scale, approximated by the largest fire ball, l_L is the flame thickness, calculated by the thickness of the OH signal, S_L is the laminar flame speed of the fuel, and v is the average velocity, or the average jet speed. Parameters v, L from Eq. 1 and l_0, l_L, v from Eq. 2 can be measured from these experiments. The 3D OH PLIF technique is better suited for measuring the parameters than 2D OH PLIF, because the uncertainty is reduced.

The 3D OH PLIF is well applicable to gelled droplet combustion because 1000 Hz is adequate repetition rate and produces enough slices to view these dynamic events. If, however, a frequency of interest in another combustion flow field is greater than 500Hz, the 3D temporal resolution of 1 ms would be insufficient.

4. Conclusion

A 3D OH PLIF was assembled and demonstrated using 5 kHz OH PLIF system and 500 Hz galvanometric mirror sweeping in triangle wave. A 3D time resolution of 1 ms was achieved, with five slices generated per sweep. The number of slices can be increased, at a decreased time resolution. Since the identification of transient flame patterns is facilitated by the ability to visualize the flame front at multiple planes, the 3D OH PLIF technique offers

great promise for combustion events diagnostic. The system is limited by the repetition rate of the pulsed laser, which is 5 kHz in this work. In a combustion flow field with a frequency of interest over 500 Hz, dynamic events would not be resolved.

The system was applied to 3 wt.% and 6 wt.% HPC methanol gelled droplet combustion in 1 atm, and at room temperature. The 3D OH PLIF system was able to record dynamics jetting events with sufficient time and spatial resolution. The system gave more complete picture of the complex asymmetrical and random flame structure of gelled droplet combustion. Previous visual observation with 2D OH PLIF indicated that a fire ball that was detached from the flame sheet. With the 3D OH PLIF, it is shown that the fire ball is actually attached to the flame sheet with a thin stretched flame. The 3D system is expected to give more accurate measurement of flame standoff distance, flame sheet thickness, position and velocity of jetting event, than its 2D counterpart.

Future work includes modeling the flame disruption, broken flame front, and fireball formation in gelled droplet combustion. Some non-premixed turbulent jet combustion models may be applicable to the jetting events in gelled droplet combustion to determine criterions for local flame extinction and fireball formation. The 3D OH PLIF data is crucial for developing accurate models. More 3D OH PLIF measurements of gelled droplet combustion will be made, as well as other multiphase combustion systems.

Acknowledgement

The research presented in this paper was made possible with the financial support of the U.S. Army Research Office under the Multi-University Research Initiative (MURI) grant number W911NF-08-1-0171 with Dr. Ralph A. Anthenien Jr. as program manager. The author would like to thank Sarah Isert for their invaluable assistances and advices.

References

1. Arnold, R., and Anderson, W. E. "Droplet Burning of JP-8/Silica Gels," *48th AIAA Aerospace Sciences Meeting Including the New Horizons Forum and Aerospace Exposition*. American Institute of Aeronautics and Astronautics, 2010, AIAA 2010-421. doi:10.2514/6.2010-421

2. Arnold, R., Santos, P. H. S., deRidder, M., Campanella, O. H., and Anderson, W. E. "Comparison of Monomethylhydrazine/ Hydroxypropylcellulose and Hydrocarbon/Silica Gels," *48th AIAA Aerospace Sciences Meeting Including the New Horizons Forum and Aerospace Exposition*. American Institute of Aeronautics and Astronautics, 2010, AIAA 2010-422. 10.2514/6.2010-422

3. Boxx, I., Stöhr, M., Carter, C., and Meier, W. "Sustained multi-kHz flamefront and 3-component velocity-field measurements for the study of turbulent flames," *Applied Physics B* Vol. 95, No. 1, 2009, pp. 23-29. doi: 10.1007/s00340-009-3420-4

4. Cho, K. Y., Pourpoint, T. L., Son, S. F., and Lucht, R. P. "Microexplosion investigation of organic MMH gel droplet with 5 kHz OH PLIF," Submitted to *Journal of Propulsion and Power*, 2013.

5. Crimaldi, J. P. "Planar laser induced fluorescence in aqueous flows," *Experiments in Fluids* Vol. 44, No. 6, 2008, pp. 851-863. doi: 10.1007/s00348-008-0496-2

6. Crimaldi, J. P., and Koseff, J. R. "High-resolution measurements of the spatial and temporal scalar structure of a turbulent plume," *Experiments in Fluids* Vol. 31, No. 1, 2001, pp. 90-102. doi: 10.1007/s003480000263

7. Deusch, S., and Dracos, T. "Time resolved 3D passive scalar concentration-field imaging by laser induced fluorescence (LIF) in moving liquids," *Measurement Science and Technology* Vol. 12, No. 2, 2001, p. 188. doi:10.1088/0957-0233/12/2/310

8. Hanson, R. K., Seitzman, J. M., and Paul, P. H. "Planar laser-fluorescence imaging of combustion gases," *Applied Physics B: Lasers and Optics* Vol. 50, No. 6, 1990, pp. 441-454. doi: 10.1007/bf00408770

9. Hedman, T. D., Cho, K. Y., Satija, A., Groven, L. J., Lucht, R. P., and Son, S. F. "Experimental observation of the flame structure of a bimodal ammonium perchlorate composite propellant using 5kHz PLIF," *Combustion and Flame* Vol. 159, No. 1, 2012, pp. 427-437. doi: 10.1016/j.combustflame.2011.07.007

10. Hedman, T. D., Groven, L. J., Cho, K. Y., Lucht, R. P., and Son, S. F. "The diffusion flame structure of an ammonium perchlorate based composite propellant at elevated pressures," *Proceedings of the Combustion Institute* Vol. 34, No. 1, 2013, pp. 649-656. doi: http://dx.doi.org/10.1016/j.proci.2012.06.171

11. Hedman, T. D., Reese, D. A., Cho, K. Y., Groven, L. J., Lucht, R. P., and Son, S. F. "An experimental study of the effects of catalysts on an ammonium perchlorate based composite propellant using 5 kHz PLIF," *Combustion and Flame* Vol. 159, No. 4, 2012, pp. 1748-1758. doi: http://dx.doi.org/10.1016/j.combustflame.2011.11.014

12. Hult, J., Meier, U., Meier, W., Harvey, A., and Kaminski, C. F. "Experimental analysis of local flame extinction in a turbulent jet diffusion flame by high repetition 2-D laser techniques and multi-scalar measurements," *Proceedings of the Combustion Institute* Vol. 30, No. 1, 2005, pp. 701-709. doi: 10.1016/j.proci.2004.08.069

13. Kaminski, C. F., Hult, J., and Aldén, M. "High repetition rate planar laser induced fluorescence of OH in a turbulent non-premixed flame," *Applied Physics B: Lasers and Optics* Vol. 68, No. 4, 1999, pp. 757-760. doi: 10.1007/s003400050700

14. Kunin, A., Natan, B., and Greenberg, J. B. "Theoretical Model of the Transient Combustion of Organic-Gellant-Based Gel Fuel Droplets," *Journal of Propulsion and Power* Vol. 26, No. 4, 2010, pp. 765-771. doi: 10.2514/1.41705

15. Kychakoff, G., Paul, P. H., van Cruyningen, I., and Hanson, R. K. "Movies and 3-D images of flowfields using planar laser-induced fluorescence," *Appl. Opt.* Vol. 26, No. 13, 1987, pp. 2498-2500. doi: 10.1364/AO.26.002498

16. Meneveau, C., and Poinsot, T. "Stretching and quenching of flamelets in premixed turbulent combustion," *Combustion and Flame* Vol. 86, No. 4, 1991, pp. 311-332. doi: http://dx.doi.org/10.1016/0010-2180(91)90126-V

17. Mercier, X., Orain, M., and Grisch, F. "Investigation of droplet combustion in strained counterflow diffusion flames using planar laser-induced fluorescence," *Applied Physics B* Vol. 88, No. 1, 2007, pp. 151-160. doi: 10.1007/s00340-007-2605-y

18. Müller, S. H. R., Böhm, B., Gleißner, M., Arndt, S., and Dreizler, A. "Analysis of the temporal flame kernel development in an optically accessible IC engine using high-speed OH-PLIF," *Applied Physics B* Vol. 100, No. 3, 2010, pp. 447-452. doi: 10.1007/s00340-010-4134-3

19. Natan, B., and Rahimi, S. "The Status of Gel Propellants in Year 2000," Vol. 5, No. 1-6, 2002, pp. 172-194. doi: 10.1615/IntJEnergeticMaterialsChemProp.v5.i1-6.200

20. Paa, W. "Combined multispecies PLIF diagnostics with kHz rate in a technical fuel mixing system relevant for combustion processes," Vol. 5880, 2005, pp. 58800N-58800N-8. doi: 10.1117/12.616769

21. Solomon, Y., Natan, B., and Cohen, Y. "Combustion of gel fuels based on organic gellants," *Combustion and Flame* Vol. 156, No. 1, 2009, pp. 261-268. doi: 10.1016/j.combustflame.2008.08.008

22. Tian, X., and Roberts, P. W. "A 3D LIF system for turbulent buoyant jet flows," *Experiments in Fluids* Vol. 35, No. 6, 2003, pp. 636-647.
doi: 10.1007/s00348-003-0714-x

23. Unger, D. R., and Muzzio, F. J. "Laser-induced fluorescence technique for the quantification of mixing in impinging jets," *AIChE Journal* Vol. 45, No. 12, 1999, pp. 2477-2486.
doi: 10.1002/aic.690451203

24. Van Vliet, E., Van Bergen, S. M., Derksen, J. J., Portela, L. M., and Van den Akker, H. E. A. "Time-resolved, 3D, laser-induced fluorescence measurements of fine-structure passive scalar mixing in a tubular reactor," *Experiments in Fluids* Vol. 37, No. 1, 2004, pp. 1-21.
doi: 10.1007/s00348-004-0779-1

25. Wellander, R., Richter, M., and Aldén, M. "Time resolved, 3D imaging (4D) of two phase flow at a repetition rate of 1 kHz," *Opt. Express* Vol. 19, No. 22, 2011, pp. 21508-21514.
doi: 10.1364/OE.19.021508